Ab initio volume-dependent elastic and lattice dynamical properties of chalcopyrite $CuGaSe_2$

Cihan Parlak and Resul Eryiğit
Department of Physics, Abant Izzet Baysal University, Bolu-14280, Turkey
(Received 4 April 2006; revised manuscript received 24 May 2006; published 29 June 2006)

We report the results of a first principles study of volume-dependent elastic and lattice dynamical properties of chalcopyrite semiconductor $CuGaSe_2$. The calculations have been carried out within density-functional perturbation theory framework, employing the local density functional approximation with norm-conserving pseudopotentials and a plane-wave basis set. Born effective charge tensors, dielectric permittivity tensors, the phonon frequencies at the Brillouin zone center and their Grüneisen parameters are calculated by using density functional perturbation theory while the elastic constants are calculated in metric-tensor formulation. We compared the Grüneisen parameters of the calculated quantities to those of ZnSe which is the isoelectronic analog of $CuGaSe_2$ and other zinc-blende-type materials and found similar trends.

DOI: 10.1103/PhysRevB.73.245217 PACS number(s): 63.20.Dj, 62.20.Dc, 77.22.Ch, 78.30.Hv

I. INTRODUCTION

Copper-based chalcopyrites $Cu(In,Ga)Se_2$ are considered to be a promising class of materials for solar-cell applications with a proven efficiency of 18.8%.[1] One way of improving the efficiency of these cells is the use of tandem structures. $CuGaSe_2$-$CuInSe_2$ structure with high band gap (E_g) $CuGaSe_2$ (E_g=1.68 eV) on top of low gap $CuInSe_2$ (E_g=1.0 eV) would form an ideal couple for tandem photovoltaic applications.[2] Structural, electronic, and lattice dynamical properties of both of these materials have been widely studied for the last three decades by a number of experimental and theoretical methods. However, there are still inconsistencies among the reported experimental results especially concerning the lattice dynamical properties which were the subject of recent theoretical work for $CuInSe_2$.[3,4]

The study of characteristic phonon frequencies is one of the most important methods for the characterization of strained materials. Pressure dependence of lattice dynamical properties, such as effective charges, phonon frequencies, and low frequency dielectric constants provide crucial information about the structure of the material. Shifted phonon frequencies are signatures of strain state of the material and can be used to clarify mode structure by Raman scattering. Elastic properties of the material are another important ingredient of such an investigation. Elastic constants of most of the chalcopyrite family of semiconductors have not been determined experimentally because of various difficulties in growing single crystals of these compounds.[5] The availability of reliable elastic constant data is an essential prerequisite for any calculation or analysis of the influence of pressure, stress, and strain on the properties of crystals and thin epitaxial layers.

The aim of the present work is to use a first principles linear response approach to delineate the lattice dynamical properties, such as Brillouin zone center phonon frequencies, Born effective charge and dielectric permittivity tensors and elastic compliance tensor of chalcopyrite $CuGaSe_2$ under hydrostatic pressure. As chalcopyrite structure can be obtained from the zinc-blende structure by simple doubling and small deformations (as detailed in Sec. III A), $CuGaSe_2$ can be considered as a superstructure of ZnSe and electronic as well as lattice dynamical properties of the former could be derived from those of the latter by using a Brillouin zone folding scheme, as a first approximation. In this work, we also provide a comparison of calculated properties for these two materials and comment on the efficiency of the folding approach.

The outline of the paper is as follows. In Sec. II we briefly review the underlying computational method and the parameters of the calculations. In the following section, volume-dependent elastic compliance, effective charge, and electronic and static dielectric tensors, zone center phonon frequencies are presented and compared to the experiments and tetrahedral binary compounds. Section IV concludes the paper with a brief review of the main results.

II. COMPUTATIONAL DETAILS

All of the results reported in this paper were obtained by using ABINIT (Ref. 6) implementation of the density-functional theory (DFT) and density-functional perturbation theory (DFPT) with a plane-wave basis set for the electronic wave functions and periodic boundary conditions. The interaction between the valence electrons and the nuclei and core electrons is described by Troullier-Martins-type norm-conserving pseudopotentials. The details of these pseudopotentials were reported before for calculations on $CuInSe_2$,[3] $CuGaS_2$,[7] and $CuInS_2$,[8] and will not be discussed here. The exchange-correlation energy is evaluated in local density approximation (LDA), using Perdew-Wang parametrization[9] of Ceperley-Alder electron-gas data.[10] A kinetic energy cutoff of 45 Ha for the plane-wave expansion and a 12 special k-point sampling for the Brillouin zone integration was found to be enough for the convergence of the total energy (to 0.01 eV) as well as the response quantities (to 1%).

Lattice dynamical and elastic properties are calculated within the framework of density functional perturbation theory.[11] Technical details of the computation of responses to strain perturbations, atomic displacements, and homogeneous electric fields can be found in Refs. 12 and 13 while Ref. 14 presents the subsequent computation of dynamical matrices, Born effective charges, dielectric permittivity tensors, and interatomic force constants. The details of the cal-

TABLE I. Calculated structural parameters of $CuGaSe_2$ compared to experimental data (a in a.u., η and u are dimensionless).

	This work	Ref. 15	Ref. 16	Ref. 17
a	10.274	10.610	10.619	10.597
η	1.971	1.965	1.963	1.972
u	0.270	0.250	0.255	—

culation of elastic constants in the linear response framework are given in Ref. 13.

III. RESULTS

A. Atomic structure and lattice properties

The chalcopyrite structure can be derived from the well-known zinc-blende structure by doubling the latter unit cell in the z direction and populating one of the fcc cubic sublattice with group VI atoms and the other one with equal amounts of groups I and III atoms in a regular fashion. Since, generally, I-VI and III-VI bond lengths, denoted by $d_{\text{I-VI}}$ and $d_{\text{III-VI}}$, respectively, are not equal, mentioned substitution results in two different structural deformations: the first one is the relocation of anions in the x-y plane which is characterized by parameter $u=0.25+(d^2_{\text{I-VI}}-d^2_{\text{III-VI}})/a^2$. Here, a is the lattice constant in the x or y direction. The second consequence of differing anion-cation bond lengths is a deformation of the unit cell along the z axis to a length c which is generally different from $2a$. This tetragonal distortion is characterized by the quantity $\eta=c/a$. The resulting structure is body-centered tetragonal with space group D^{12}_{2d} (No. 122).

The ground-state properties in the pressure-free case are obtained by minimization of total energy with respect to the unit cell volume V. This is done by calculating the total energy for a number of fixed η values. For each η, u is determined by minimizing the force on the atoms. The hydrostatic pressure is simulated by a uniform decrease in lattice constants a and c. For each compressed volume, u is recalculated from the force considerations.

The zero pressure lattice structural properties are obtained by energy and force minimization and compared to the available experimental values in Table I. Considering the fact that the zero-point motion and thermal effects are not taken into account, the calculated a, η, and u values agree with the experimental values quite well. Since it is found that $u>0.25$, the Ga-Se bond is slightly shorter than the Cu-Se bond. The bulk modulus and its pressure derivative calculated by fitting to a third-order Vinet equation of state[18] are found to be 84.5 GPa and 4.7 which are in good agreement with available experimental bulk modulus values of $CuGaSe_2$ [75.67,[19] 70.18,[20] and 69.31 (Ref. 21)], but far off compared to the value 57.84 GPa reported by Ref. 22. ZnSe which is isoelectonic analog of $CuGaSe_2$ has slightly larger lattice constant $a=10.7106$ a.u. and lower bulk modulus ($B=64.7$ GPa).[23]

Under pressure tetrahedrally coordinated chalcopyrite compounds undergo transformation to a denser phase with octahedral coordination,[24] probably rock-salt structure. The phase transition pressure for $CuGaSe_2$ is around 12.5 GPa.[25] This pressure corresponds to a volume reduction of 15% if we use our calculated B_0 and B_0' values in the Vinet equation of state. Our calculations are done for the volume compression range (up to 10%) which is far away from the phase transition point.

TABLE II. Elastic constants in units of GPa.

		C_{11}	C_{12}	C_{13}	C_{33}	C_{44}	C_{66}
$CuGaSe_2$	This work	112.2	66.4	68.1	113.2	48.4	48.5
$CuInSe_2$	This work	96.8	60.9	63.2	97.0	39.1	37.9
$CuInSe_2$	Ref. 27 (Expt.)	97.0	59.7	86.0	108.9	36.2	31.6
$CuInSe_2$	Ref. 4 (Theor.)	71.0	45.3	45.3	63.3	45.5	47.4

B. Elastic constants

There are a number of ways to calculate the elastic coefficients of a material from the first principles. Until recently, the most widely used method was to deform the crystal from its equilibrium shape by a set of tetragonal and sheer deformations of various sizes and compute the resulting stress by using the quantum mechanical definition of stress.[26] The relationship between the applied strain and the calculated stress components provides a set of over-determined linear systems which are solved by a singular value decomposition to obtain sought elastic stiffness constants. Recently, Hamann *et al.*[13] developed a reduced coordinate metric tensor method for a linear response formulation of strain-type perturbations which could be calculated in DFPT. The elastic constants reported in this paper are obtained by the method of Ref. 13 as implemented in ABINIT.

The elastic stiffness tensor of chalcopyrite compounds has six independent components because of the symmetry properties of D^{12}_{2d} space group, namely $C_{11}, C_{33}, C_{44}, C_{66}, C_{12}, C_{13}$ in Young notation. The elastic compliance tensor elements of $CuGaSe_2$ which are calculated by using the method of metric tensor formulation of Hamann *et al.*[13] are displayed in Table II. Elastic stiffness tensor components must satisfy certain relations known as Born stability criteria[28] which for the tetragonal chalcopyrite lattice requires that $C_{11}, C_{33}, C_{44}, C_{66}>0$, $C_{11}>|C_{12}|$, $C_{11}C_{33}>C^2_{13}$, $(C_{11}+C_{12})C_{33}>2C^2_{13}$. The values reported in Table II satisfy all of these constraints. Since the experimental values are not available for $CuGaSe_2$, to give an idea about the expected experimental-theoretical spread, we display experimental, theoretical, and our calculated values for $CuInSe_2$ in the same table. Except for C_{13} ($\approx$25% underestimated) and C_{66} ($\approx$20% overestimated), the agreement between the calculated and experimental values is very good. The results obtained in this work seems to be much closer to the experimental values compared to those reported in Ref. 4. The main ingredients of calculations in this work and Ref. 4 are similar, namely pseudopotential LDA-DFT. Although the method of elastic constant calculations are different, results should converge to a common value. The pronounced difference in the results of these two sets of calculations might be due to lack of enough conver-

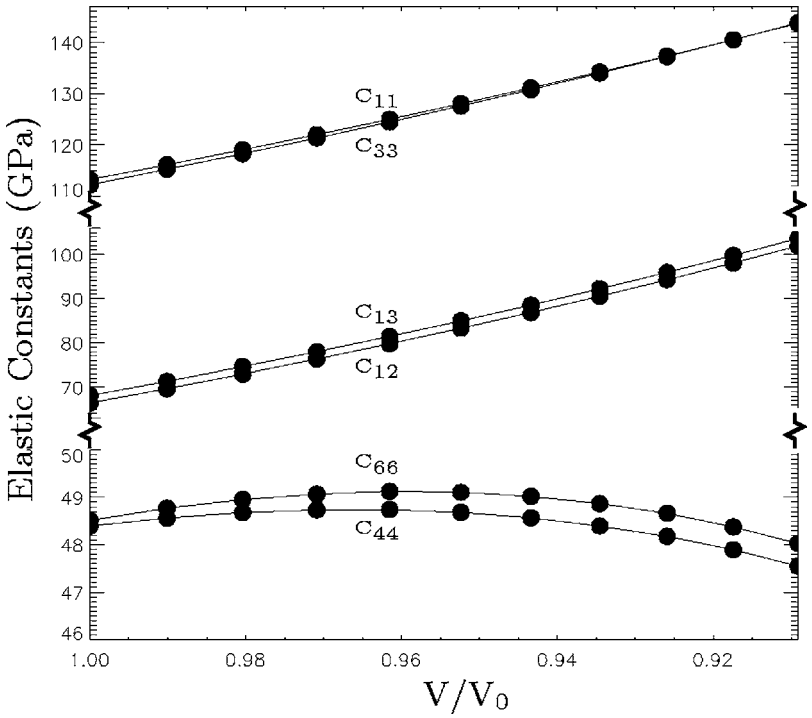

FIG. 1. Volume dependence of the components of elastic tensor of $CuGaSe_2$.

gence in the calculations reported in Ref. 4. Elastic constants reported in Table II shows that $CuGaSe_2$, also, displays pseudocubic elastic behavior: for cubic crystals $C_{11}/C_{33}=C_{44}/C_{66}=C_{12}/C_{13}=1$, from Table II we find $C_{11}/C_{33}=0.99, C_{44}/C_{66}=1.00, C_{12}/C_{13}=0.98$ for $CuGaSe_2$. A similar behavior, which is an expected result because of the u and η deformations being so small, was found for other Cu-based chalcopyrites in Ref. 4.

The volume dependence of elastic constants is displayed in Fig. 1. As can be seen from the figure, C_{44} and C_{66} increase linearly near zero pressure and then decrease almost linearly at higher pressures while the other elastic tensor components increase with the compression of the lattice. Although the pressure dependence of elastic constants of $CuGaSe_2$ is not available experimentally, elastic constants of a similar compound $CdGaAs_2$ show similar properties at low pressures.[5] Comparing the pressure behavior of elastic constants of $CuGaSe_2$ with those of its binary electronic analog ZnSe, we find a similar trend. Our calculated $P=0$ pressure derivatives $dC_{11}/dp=3.74$, $dC_{33}/dp=4.00$, $dC_{12}/dp=4.00$, $dC_{13}/dp=3.58$, $dC_{44}/dp=0.21$, and $dC_{66}/dp=0.32$ are comparable to the similar experimental values of $dC_{11}/dp=4.77$, $dC_{12}/dp=4.44$, and $dC_{44}/dp=0.43$ for ZnSe. An interesting point that can be observed from the pressure-dependent C_{ij}s is that after a volume reduction of 8%, dC_{44}/dp and dC_{66}/dp become negative. This behavior is also observed for the C_{44} component of ZnSe and is thought to be related to the structural phase transition at elevated pressures. As it also can be observed from the figure, reduction of the cubic symmetry of the zinc blende to tetragonal symmetry of chalcopyrite structure increases the number of independent coefficients of the elasticity tensor from three to six. However, because of the smallness of the tetragonal distortion the splittings of $C_{11}-C_{33}$, $C_{12}-C_{13}$, and $C_{44}-C_{66}$ are very small.

One can define linear compressibilities for the pressure response of lattice constants a (κ_a) and c (κ_c) axis of chalcopyrite structure.[5] κ_a and κ_c can be expressed in terms of elastic stiffness constants as

$$\kappa_a = -\frac{1}{a}\frac{\partial a}{\partial p} = \frac{C_{33}-C_{13}}{C_{33}(C_{11}+C_{12})-2C_{13}^2},$$

$$\kappa_c = -\frac{1}{c}\frac{\partial c}{\partial p} = \frac{C_{11}+C_{12}-2C_{13}}{C_{33}(C_{11}+C_{12})-2C_{13}^2}.$$

Our calculated κ_a and κ_c are equal to 4.1 and 3.9 TPa^{-1}, respectively. This finding partly justifies treating the effect of hydrostatic pressure on the lattice as a uniform contraction of both the a and c axis. Volume compressibility, which is defined as $\kappa=2\kappa_a+\kappa_c$, is equal to 12.1 TPa^{-1}, which is similar to that reported for other chalcopyrite compounds.[5]

The volume dependence of κ_a and κ_c and the bulk modulus are displayed in Fig. 2. As expected, compressibilities along the a and c axis decrease linearly with pressure while the bulk modulus increases.

C. Born effective charges

Born effective charge tensors determine, with the electronic permittivity tensor ϵ_∞, the strength of Coulomb interaction which is responsible for the splitting between the transverse (TO) and the longitudinal (LO) optical modes for insulators. It is a measure of the change in electronic polarization due to ionic displacements. For atom κ, $Z^{\star}_{\kappa,\beta\alpha}$ quantifies to linear order the polarization per unit cell, created along the direction β when the atoms of sublattice κ are displaced along the direction α, under the condition of zero electric field. Compassionately, it is the mixed second derivative of the total energy with respect to macroscopic field

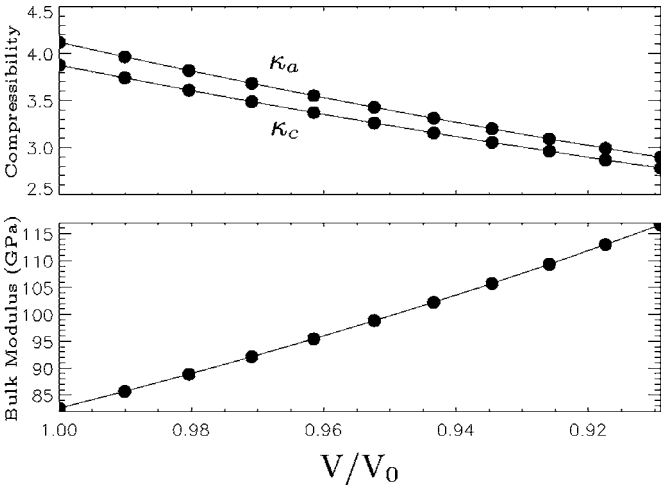

FIG. 2. Volume dependence of the bulk modulus and a and c axis compressibilities of $CuGaSe_2$.

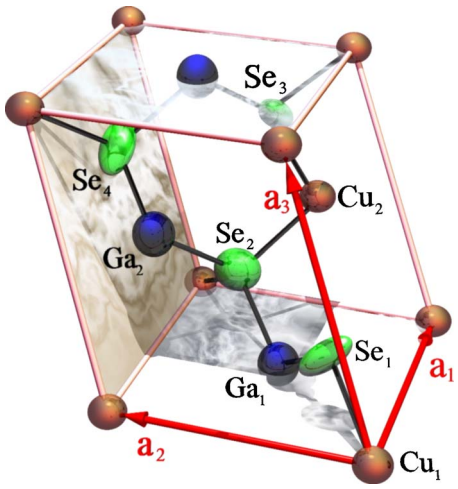

FIG. 3. (Color online) Dynamical Born effective charges of chalcopyrite $CuGaSe_2$. Here, for each atom the unit sphere is transformed by the effective charge tensor of that atom. Ga and Se spheres are further scaled by 1/3 and 1/2, respectively, for visual clarity.

component E_α and β component of the displacement of the κth particle. The form of the Born effective charge tensor for atom κ is determined by the site symmetry of the position of that atom in the lattice. Eight atoms of the primitive unit cell of the chalcopyrite structure are located in three different Wyckoff positions; Cu at $4a$ with symmetry S_4, Ga at $4b$ with symmetry S_4, and Se at $8d$ with symmetry C_2. Based on group theoretical considerations none of the $Z^\star_\kappa$s for the $CuGaSe_2$ is not expected to be diagonal for any of the atoms.

In Table III we display dynamical effective charge tensors, eigenvalues of symmetric parts of these tensors, and Grüneisen parameters of these eigenvalues, $\gamma^\star$, which is defined as

$$\gamma^\ddagger = -\frac{d \ln \lambda}{d \ln V}, \tag{1}$$

where V is the unit cell volume and λ is the eigenvalue of the symmetric part of the relevant effective charge tensor. The effective charge tensors are also displayed graphically in Fig. 3. Because of finite k-point sampling there is a deviation from charge neutrality which is less than 0.01 electron for the unit cell. The first thing to consider from Table III is that

TABLE III. Calculated Born effective charges of $CuGaSe_2$. The eigenvalues λ of the symmetric part of $Z^\star$ are given in brackets. The last column is the Grüneisen parameter $\gamma^\star$ for the effective charge.

		λ	$\gamma^\star$
$Z^\star_{Cu}$	$\begin{pmatrix} 0.72 & 0.12 & 0.00 \\ -0.12 & 0.72 & 0.00 \\ 0.00 & 0.00 & 0.64 \end{pmatrix}$	$\begin{bmatrix} 0.72 \\ 0.72 \\ 0.64 \end{bmatrix}$	$\begin{bmatrix} -3.58 \\ -3.58 \\ -3.64 \end{bmatrix}$
$Z^\star_{Ga}$	$\begin{pmatrix} 2.47 & 0.12 & 0.00 \\ -0.12 & 2.47 & 0.00 \\ 0.00 & 0.00 & 2.72 \end{pmatrix}$	$\begin{bmatrix} 2.47 \\ 2.47 \\ 2.72 \end{bmatrix}$	$\begin{bmatrix} -0.14 \\ -0.14 \\ -0.38 \end{bmatrix}$
$Z^\star_{Se_1}$	$\begin{pmatrix} -1.41 & 0.00 & 0.00 \\ 0.00 & -1.78 & 0.68 \\ 0.00 & 0.75 & -1.68 \end{pmatrix}$	$\begin{bmatrix} -2.45 \\ -1.41 \\ -1.01 \end{bmatrix}$	$\begin{bmatrix} -0.80 \\ -0.77 \\ -1.54 \end{bmatrix}$
$Z^\star_{Se_3}$	$\begin{pmatrix} -1.78 & 0.00 & 0.68 \\ 0.00 & -1.41 & 0.00 \\ 0.75 & 0.00 & -1.68 \end{pmatrix}$	$\begin{bmatrix} -2.45 \\ -1.41 \\ -1.01 \end{bmatrix}$	$\begin{bmatrix} -0.80 \\ -0.77 \\ -1.54 \end{bmatrix}$

compared to nominal charges of Cu, Ga, and Se in $CuGaSe_2$ (+1, +3, and −2, respectively), the dynamical charges show no anomalous behavior which is expected because such anomalous effective dynamical charges are observed for ferroelectricity unstable semiconductors as well as near metallic and strongly correlated electronic systems[29] and $CuGaSe_2$ has none of these properties. A similar trend is observed for the other $CuXY_2$ chalcopyrites where X=Al, Ga, In and Y =S and Se.

$Z^\star$ of cations, which are located at 4*a* and 4*b* Wyckoff positions, are almost diagonal with an anisotropy of ≈12.5% for Cu and ≈−9.2% for Ga. These anisotropies are higher than those seen in $CuAlS_2$,[30] but still low enough that the shapes of Cu and Ga in Fig. 3 are still almost spherical. The shape of $Z^\star$ for Se ions is markedly different from that of cations as can be seen from Table III and Fig. 3. Se ions are located at lower symmetry sites (8*d* Wyckoff positions) and as a result their effective charge tensors have nonequivalent diagonal components as well as sizable off-diagonal components. The tetrahedral shifting of anion atoms creates four different configurations for these atoms and the resulting effective charge tensor elements can be divided into two classes according to the direction of the tetrahedral shifting being along x or y direction. $Z^\star_{\mathrm{Se},zz}=-1.68$ for all anions while $Z^\star_{\mathrm{Se},xx}$ and $Z^\star_{\mathrm{Se},yy}$ take the value −1.41 or −1.78 depending on the direction of u. Also, depending on the u distortion being along x or y direction, the off-diagonal components $Z^\star_{\mathrm{Se},zx}$, $Z^\star_{\mathrm{Se},xz}$ or $Z^\star_{\mathrm{Se},yz}$, $Z^\star_{\mathrm{Se},zy}$ are different than zero. Hence, the shape of effective charge tensor for anions is far from being spherical, which also has been observed for other members of the Cu-based chalopyrite family of semiconductors.

As can be seen from the Table III, the Grüneisen parameter for the dynamical effective charges of all the ions are negative, which indicate that $Z^\star$ decreases with increasing pressure. The eigenvalues of the symmetric part of the effective charge tensors are displayed as a function of the volume in Fig. 4. The most important conclusion from the effective charge Grüneisen parameters in Table III and the graphs in Fig. 4 is that the Born effective charges decrease linearly with pressure in the considered pressure range. Pressure-induced reduction of effective charges indicates a charge redistribution in comparison with zero pressure situation and is found to be the case for almost all zinc-blende materials, except SiC.[31]

D. Dielectric permittivity tensors

Contrary to the effective charges, the form of the dielectric tensor is determined by the symmetry of the crystal and is expected to be diagonal for the chalcopyrite structure: both electronic (ϵ_∞) and static (ϵ_0) dielectric tensors should have two independent components $\epsilon^\parallel$ and $\epsilon^\perp$ along and perpendicular to the c axis, respectively. We display our calculated dielectric tensor components along with model calculations of Ref. 35 and experimentally available values in Table IV. The averages of ϵ_∞ and ϵ_0, obtained from the expression ϵ_∞ (or ϵ_0)$=(2\epsilon_\infty^\perp+\epsilon_\infty^\parallel)/3$ are also shown in this table. While electronic dielectric tensor is almost isotropic, ϵ_0 has a small (≈4.0%) anisotropy, which is consistent with the fact that

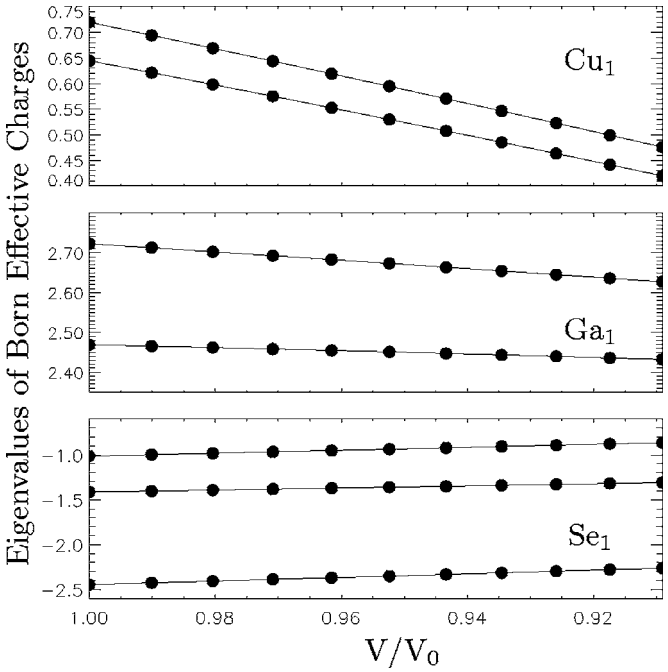

FIG. 4. Volume-dependent Born effective charges of $CuGaSe_2$.

for $CuGaSe_2$ tetragonal distortion is very small ($\eta=c/a$ ≈2).

The experimental infrared data for the electronic part of the dielectric tensor of $CuGaSe_2$ are similar and around 5, but for the static $\epsilon_0^\perp$ component there is ≈50% difference between the values reported in Ref. 32 and Ref. 34. We have performed a refitting of the reflectance data of Ref. 34 and found that the dielectric tensor components displayed in the last row of Table IV would provide a much better fit. It should be noted that these values are obtained by fitting to the sum form of the model dielectric function which is the same form as used in Ref. 34. We have found that an even better fit can be obtained by using the product form of model dielectric function with similar ϵ_∞ components. As can be seen from Table IV, our electronic computed dielectric components agree the most with the refitted values derived from the infrared reflectance data of Ref. 34: our theoretical ϵ_∞ values are ≈15% higher than the experimental values. The overestimation of the calculation is a well-known artifact of the density-functional theory (DFT) which is related to underestimation of the band gap in DFT.[36–38]

TABLE IV. Static and high frequency dielectric tensor components of $CuGaSe_2$.

	$\epsilon_\infty^\parallel$	$\epsilon_\infty^\perp$	ϵ_∞	$\epsilon_0^\parallel$	$\epsilon_0^\perp$	ϵ_0
This work	9.19	9.32	9.28	11.31	10.86	11.01
Ref. 32	4.75	6.50	5.92	6.08	8.45	7.66
Ref. 33	4.2	5.1	4.8	6.31	7.4	7.04
Ref. 34	4.20	5.13	4.82	7.30	12.86	11.01
Ref. 35	6.6	6.8	6.7	9.5	9.7	9.6
Ref. 34[a]	8.11	7.17	7.48	12.38	14.40	13.73

[a]Refitted Ref. 34 data.

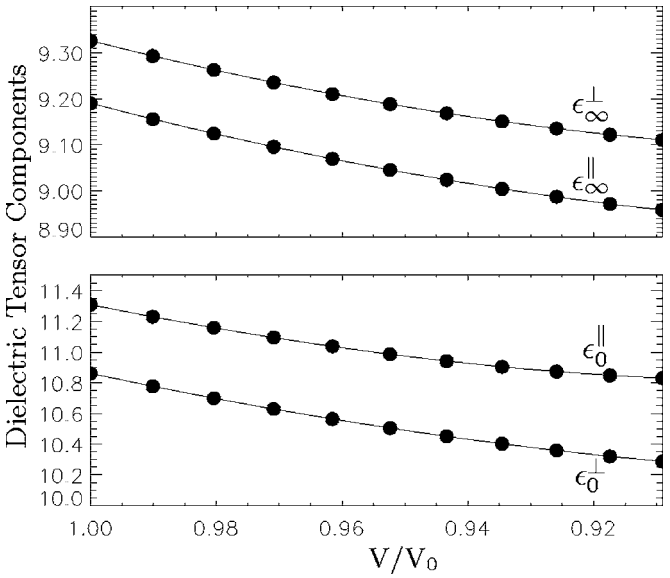

FIG. 5. Volume-dependent static and high frequency dielectric tensor components of $CuGaSe_2$.

Similar to that of Born effective charges, one can define a dielectric Grüneisen parameter

$$\gamma^{\epsilon} = -\frac{d \ln \epsilon}{d \ln V} \tag{2}$$

to characterize the pressure dependence of the dielectric constants. For $CuGaSe_2$, we have found that the perpendicular and parallel components of γ^{ϵ_∞} are both negative with a similar Grüneisen parameter ($\gamma^{\epsilon_\infty^\parallel} = -0.390$, $\gamma^{\epsilon_\infty^\perp} = -0.372$) which is similar to γ^{ϵ_∞} for zinc-blende compounds.[31] The Grüneisen parameters for the components of static dielectric function ϵ_0 are also all negative with higher absolute values compared to those of high-frequency components ($\gamma^{\epsilon_0^\perp} = -0.731$, $\gamma^{\epsilon_0^\parallel} = -0.811$, $\gamma^{\epsilon_0} = -0.784$). These values are also around those values reported for zinc-blende compounds.[31] Figure 5 displays our calculated volume-dependent static and high-frequency dielectric tensor components. All of the components decrease under pressure; the volume dependence of static (high-frequency) components is slightly (highly) nonlinear, especially at higher pressures, which is similar to what has been found for the most tetrahedrally coordinated semiconductors.

E. Zone center phonons

The unit cell of the chalcopyrite structure is almost twice the volume of zinc-blende one, with the Brillouin zone being four times smaller than that of the cubic structure. As a result, Γ, X, and W symmetry points of zinc-blende Brillouin structure zone fold to Γ of the chalcopyrite structure. Since the body-centered tetragonal primitive unit cell of the chalcopyrite structure has eight atoms (see Fig. 3), the number of vibrational modes for this structure is 24. A detailed discussion of group theoretical properties of chalcopyrite zone center phonons can be found in Ref. 53. The irreducible representation at the center of the Brillouin zone is

$$\Gamma_{\text{aco}} = 1\Gamma_4 \oplus 1\Gamma_5$$

for acoustic modes, and

$$\Gamma_{\text{opt}} = 1\Gamma_1 \oplus 2\Gamma_2 \oplus 3\Gamma_3 \oplus 3\Gamma_4 \oplus 6\Gamma_5$$

for optical modes. All the optical modes, except Γ_2, are Raman active while only Γ_4 and Γ_5 modes are infrared active. Both Γ_4 and Γ_5 modes belong to vector transforming representation, and inclusion of the long-range polarization interaction results in splitting of these modes into TO and LO components giving nine polar vibrations [three with polarization along c (Γ_4 modes) and six along x or y (Γ_5)]. This results in different numbers of IR modes being active for $E \| c$ and $E \perp c$.

Optical modes of Γ_1 and Γ_2 symmetry involve displacement of only anions while the other optical modes include displacement of cations as well. The infrared active Γ_4 mode involves in-phase motion of each cation pair and that of two anion pairs along the principal axis and as a result has a dipole moment in that direction. For the infrared active Γ_5 mode, the resultant motion of each cation pair and that of each anion pair are along either of x and y axis which causes twofold degeneracy and a dipole moment in the x-y plane. Γ_1 and Γ_3 modes are out of phase motion of ions and they do not have a dipole moment, so they are Raman active but not infrared active. Γ_2 mode is out-of-phase motion of anion pairs and does not produce a dipole moment.

Our calculated zone center phonon frequencies, their symmetry assignments, and mode Grüneisen parameters are displayed and compared with infrared[32–34,39] and Raman[40–47] spectroscopic measurements in Table V. Among the experimental phonon frequencies, Raman data of Rámirez and Rincón[42] and González and Cherrin[43] and infrared data of Syrbu *et al.*[34] are the most complete sets. The zone center phonon frequencies of Cu-based chalcopyrite semiconductors, generally, are clearly grouped into three groups: low, medium, and high frequency. As can be seen from Table V for $CuGaSe_2$ these groups are low: 65–97 cm^{-1}; medium: 170–223 cm^{-1}; and high: 265–295 cm^{-1}. Γ_1 mode which involves the motion of only the anions is always the strongest line observed in the Raman scattering of Cu-based chalcopyrite compounds and because of that its frequency is well established for $CuGaSe_2$ in the range 182–187 cm^{-1} which can be seen from the Table V. Our calculated value for this mode is 197 cm^{-1} which is in good agreement with the experimental values. Although there are some discrepancies among the experimental data for almost every mode with the exception of Γ_1 mode, the most problematic values seem to be the Raman results of Ref. 42 for the high-frequency Γ_3 modes. Our calculated frequencies and Raman measurements reported by Ref. 43 coupled with the results of experimental as well as computational studies on other Cu-based chalcopyrites seem to indicate that each one of three Γ_3 mode frequencies should be in the low, medium, and high frequency region. The discrepancies among experimental Γ_4 and Γ_5 mode frequencies are relatively low compared to some other Cu-based chalcopyrites and our calculated frequencies show reasonable agreement with the available values.

TABLE V. Frequencies of phonons and mode Grüneisen parameters at the Γ point (ω in cm^{-1}).

Mode	*Ab initio* Present	Experiment													γ_i Present
		IR[39]	IR[32]	IR[33]	IR[34]	R[47]	R[47a]	R[41]	R[46]	R[42]	R[43]	R[40]	R[44]	R[45]	
Γ_1	197					187	188	188	184	180,185	183	182	185	187	1.5
Γ_2	223														1.3
Γ_2	189														1.5
Γ_3	270									128,130	263				1.5
Γ_3	187							192	116	108,110	165				1.7
Γ_3	95								96	90,94	76	93			–0.04
Γ^{LO}_{4TO}	295	278	265	273	273			265	261	259,261	278				1.3
	275	254	244	257	257			244			252				1.5
Γ^{LO}_{4TO}	210	196	194	188	188			194	199	200,202			195	199	2.1
	205	178	186	177	177			186			187				2.2
Γ^{LO}_{4TO}	87			96	96			60	60	68	98	57			–0.3
	86			86	86			60			98				–0.4
Γ^{LO}_{5TO}	289	276	269	277	27	274	278	269	261	273	273	269	274	27	1.3
	271	250	241	255	255	249	252	241						253	1.6
Γ^{LO}_{5TO}	266			186	186				239	237,245	243	267	227	242	1.5
	265			180	180						219			238	1.4
Γ^{LO}_{5TO}	208	190	188	149	149		193	188		153,156	187	242	153		2.4
	206	170	184	145	145			184			170			193	2.4
Γ^{LO}_{5TO}	170			109	135	154	154		168	141,142	140	204			2.1
	170			105	128			156			140				2.2
Γ^{LO}_{5TO}	97			90.9	91	96	96			117,121			80	117	–0.6
	97			88.2	82	86	86	98							–0.6
Γ^{LO}_{5TO}	65			66	67.5				60	75	58		60	78	–1.8
	65			64.5	64	60	59				58			60	–1.8
		rms relative deviations													
		0.114	0.106	0.290	0.238	0.083	0.076	0.187	0.279	0.386	0.144	0.232	0.124	0.038	

[a]Reference 47 (at 77 K).

The calculated LO-TO mode splitting of Γ_4 and Γ_5 modes are small, ranging from 0 to 20 cm^{-1}. As can be observed from the Table V, the highest splitting is for the highest frequency modes for both symmetries which is also the case for the experimental data. The small and even zero splitting for the low frequency modes can be traced back to the origin of these modes: since the low frequency modes are essentially the folded acoustic modes, they correspond to whole molecular units moving relative to each other. On the other hand, the high frequency modes involve individual atoms moving against each other which produces higher dipole moments which lead to higher splitting. The highest of these splitting values are around the half of the LO-TO splitting for zone center optical mode of isoelectronic ZnSe. A similar reduction value was obtained by Lambrecnt *et al.*[48] who compared the splittings for ternary $ZnGeN_2$ and its isoelectronic analog binary GaN.

The hydrostatic pressure dependence of phonon mode i with frequency ω_i is characterized by the Grüneisen parameter γ_i which is defined as

$$\gamma_i = -\frac{d \ln \omega_i}{d \ln V}, \tag{3}$$

where V is the unit cell volume of the crystal. In Table V we also display our calculated mode Grüneisen parameters. To the best of our knowledge, there are no reported experimental Grüneisen parameters for the Γ point phonons of $CuGaSe_2$. Here, we discuss the computed results with reference to γ_iS of comparable compounds. One of the interesting properties of phonons of tetrahedrally coordinated semiconductors of diamond and zinc-blende structure is the pressure softening of their transverse acoustic (TA) modes. Mode Grüneisen parameter for TA modes of group IV, III-V, and II-VI compounds that crystallize in diamond and zinc-blende structure are all negative towards the Brillouin zone boundaries[49] and this negativity is thought to be the mechanism of structural phase transition of these compounds at elevated pressures. The correspondence between the chalcopyrite zone center phonon modes and modes in zinc-blende structure has been given in Refs. 50–53. We have

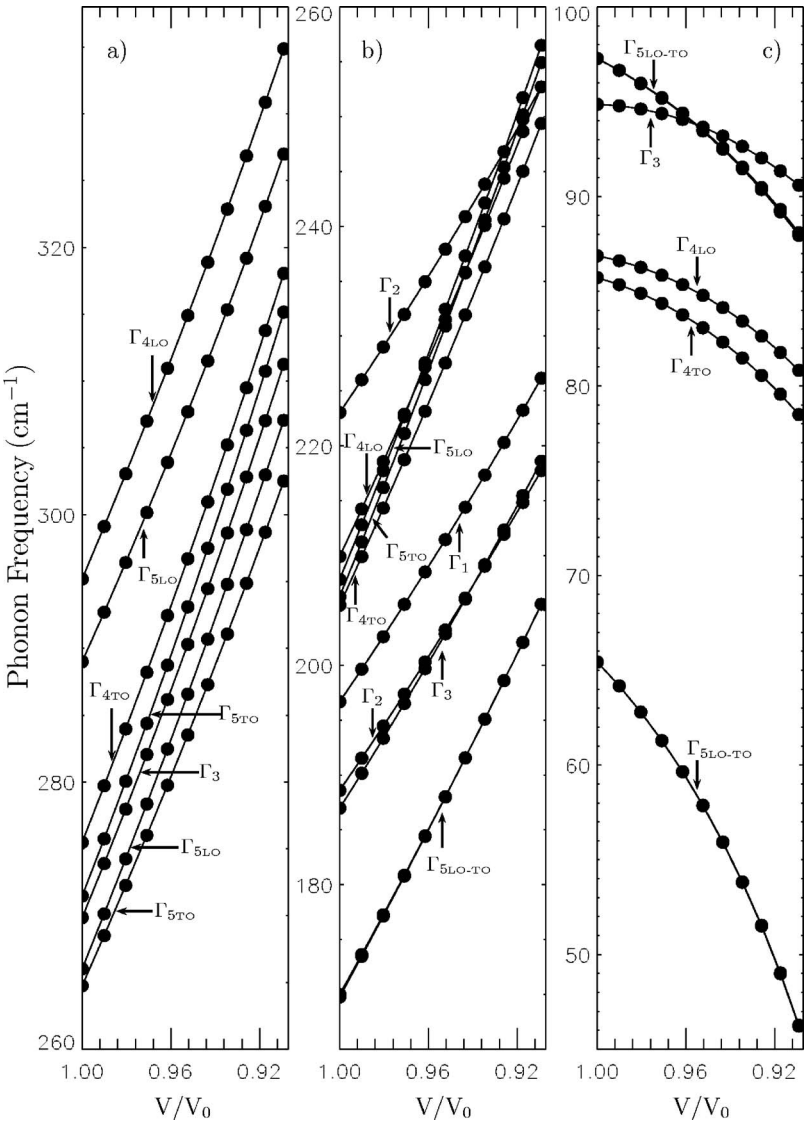

FIG. 6. Volume dependence of phonon frequencies for $CuGaSe_2$ at the Γ point.

found four negative mode Grüneisen parameters for $CuGaSe_2$, which are two low frequency optical Γ_5, one low frequency Γ_4, and one low frequency Γ_3 modes. Of these modes, Γ_3 and Γ_4 originates from the zone boundary W_2 transverse acoustic (TA) and Γ_5 modes come from zone boundary TA modes at X_{5ac}, W_{4ac} points of zinc-blende structure. Among the negative γs, the one originating from the X_{5ac} mode is the largest in magnitude which is similar to values reported for zinc-blende structures.[54–57] Frequency and mode Grüneisen parameters at W point for zinc-blende materials are, unfortunately, not as well known as those at X point. From the available data[55] we would expect a smaller, but still negative Grüneisen parameter.

For zinc-blende materials, the mode Grüneisen parameter for longitudinal optical phonon modes (γ_{TO}) is generally higher than that of transverse optical mode (γ_{LO}),[55] which is interpreted as reflection of a decrease in ionicity with increasing pressure. We have found a similar relationship for $CuGaSe_2$ for the polar modes (the highest frequency Γ_5 and Γ_4 modes) originating from the zone-center polar mode (Γ_{15}) of zinc-blende structure.

The volume-dependent zone-center phonon frequencies of $CuGaSe_2$ are shown in Figs. 6(a)–6(c) for high, medium, and low frequency modes, respectively. One noticeable feature of this figure is that all the high and medium frequency modes have a positive and linear increase while low frequency modes have a slightly nonlinear decrease with increasing pressure. Another important observation from the figure is that the pressure rate of increase for high frequency modes are similar [Fig. 6(a)]. For the medium frequency group [Fig. 6(b)] Γ_1, Γ_2, and Γ_3 modes show a similar rate of increase while the remaining modes in this group have a similar rate. The low frequency region which is displayed in Fig. 6(c) show a completely different behavior. Pressure dependence of Γ_3 and Γ_4 modes in this region are similar which is a reflection of the fact that these two modes come from the same W_2 point of the zinc-blende structure.

IV. CONCLUSION

We have investigated the pressure-dependent elastic and lattice dynamical properties of ternary semiconductor

$CuGaSe_2$ within the density functional perturbation theory framework. The pressure derivatives of the components of elastic stiffness tensor were found to be similar in magnitude and sign to those of the isoelectronic binary analog compound ZnSe; while at $P=0$ all of them are positive, at elevated pressures the pressure derivative of C_{44} and C_{66} become negative. The pressure dependence of lattice dynamical properties such as Born effective charge tensor, Brillouin zone center phonon frequencies, and static and high frequency dielectric tensors were, also, found to show similar trends with binary tetrahedrally coordinated compounds. Under hydrostatic pressure, the dynamical effective charges decrease. The zone-center modes originating from the modes with negative Grüneisen parameter in zinc-blende materials, have negative Grüneisen parameters and the ordering of $\gamma_{TO} > \gamma_{LO}$ is respected for the zone-center chalcopyrite modes that originate from the zone-center polar mode of zinc-blende structure. An overall finding from the pressure dependence of the response quantities considered in this study is the general similarity of the behavior in the chalcopyrite ternary compound and the zinc-blende binary compounds. This finding is partly expected because the local bonding and structural modification from the zinc-blende to chalcopyrite transformation is not very high as can be seen from the u (=0.27 instead of 0.25) and η (=1.97 instead of 2) values.

ACKNOWLEDGMENTS

This work was supported by Tübitak under Grant No. TBAG-2449(104T057) and AIBU Research Fund Grant No. 04.03.02.199.

[1] M. A. Contreras, B. Egaas, K. Ramanathan, J. Hiltner, A. Swartzlander, F. Hasoon, and R. Noufi, Prog. Photovoltaics **7**, 311 (1999).
[2] S. Siebentritt, A. Bauknecht, A. Gerhard, U. Fiedeler, T. Kampschulte, S. Schuler, W. Harneit, S. Brehme, and J. Albert, Sol. Energy Mater. Sol. Cells **67**, 129 (2001).
[3] C. Parlak and R. Eryiğit, Phys. Rev. B **66**, 165201 (2002).
[4] J. Lazewski, H. Neumann, P. T. Jochym, and K. Parlinski, J. Appl. Phys. **93**, 3789 (2003).
[5] H. Neumann, Cryst. Res. Technol. **39**, 939 (2004).
[6] X. Gonze, J.-M. Beuken, R. Caracas, F. Detraux, M. Fuchs, G.-M. Rignanese, L. Sindic, M. Verstraete, G. Zerah, F. Jollet, M. Torrent, A. Roy, M. Mikami, Ph. Ghosez, J.-Y. Raty, and D. C. Allan, Comput. Mater. Sci. **25**, 478 (2002). http://www.abinit.org
[7] M. Akdoğan and R. Eryiğit, J. Phys. Condens. Matter **14**, 7493 (2002).
[8] R. Eryiğit, C. Parlak, and R. Eryiğit, Eur. Phys. J. B **33**, 251 (2003).
[9] J. P. Perdew and Y. Wang, Phys. Rev. B **45**, 13244 (1992).
[10] D. M. Ceperley and B. J. Alder, Phys. Rev. Lett. **45**, 566 (1980).
[11] S. Baroni, S. de Gironcoli, A. Dal Corso, and P. Giannozzi, Rev. Mod. Phys. **73**, 515 (2001).
[12] X. Gonze, Phys. Rev. B **55**, 10337 (1997).
[13] D. R. Hamann, X. Wu, K. M. Rabe, and D. Vanderbilt, Phys. Rev. B **71**, 035117 (2005).
[14] X. Gonze and C. Lee, Phys. Rev. B **55**, 10355 (1997).
[15] H. W. Spiess, U. Heaberln, G. Brandt, A. Räuber, and J. Schneider, Phys. Status Solidi B **62**, 183 (1974).
[16] T. Martin, J. M. Merino, J. L. Martin de Vidales, M. Leon, F. Rueda, and R. Diaz, Adv. Mater. Opt. Electron. **8**, 147 (1998).
[17] J. Krustok, J. Raudoja, J.-H. Schön, M. Yakushev, and H. Collan, Thin Solid Films **361–362**, 406 (2000).
[18] P. Vinet, J. H. Rose, J. Ferrante, and J. R. Smith, J. Phys.: Condens. Matter **1**, 1941 (1989).
[19] R. R. Reddy, Y. Nazeer Ahammed, K. Rama Gopal, P. Abdul Azeem, T. V. R. Rao, and P. Mallikarjuna Reddy, Opt. Mater. **14**, 355 (2000).
[20] Q. B. Meng, C. Y. Xiao, Z. J. Wu, Ke-an Feng, Z. D. Lin, and S. Y. Zhang, Solid State Commun. **107**, 369 (1998).
[21] R. Asokamani, R. M. Amirthakumari, R. Rita, and C. Ravi, Phys. Status Solidi B **213**, 349 (1999).
[22] M. Belhadj, A. Tadjer, B. Abbar, Z. Bousahla, B. Bouhafs, and H. Aourag, Phys. Status Solidi B **241**, 2516 (2004).
[23] B. H. Lee, J. Appl. Phys. **44**, 2984 (1970).
[24] A. Werner, H. D. Hochheimer, and A. Jayaraman, Phys. Rev. B **23**, 3836 (1981).
[25] A. Kraft, G. Kühn, and K. W. Möller, Z. Anorg. Allg. Chem. **504**, 155 (2004).
[26] O. H. Nielsen and R. M. Martin, Phys. Rev. Lett. **50**, 697 (1983).
[27] R. Fouret, B. Hennion, J. Gonzalez, and S. M. Wasim, Phys. Rev. B **47**, 8269 (1993).
[28] M. Born and K. Huang, *Dynamical Theory of Crystal Lattices* (Clarendon Press, Oxford, 1954).
[29] A. Filippetti and N. A. Spaldin, Phys. Rev. B **68**, 045111 (2003).
[30] C. Parlak and R. Eryiğit, Phys. Rev. B **70**, 075210 (2004).
[31] A. Debernardi, C. Ulrich, M. Cardona, and K. Syassen, Phys. Status Solidi B **223**, 213 (2001).
[32] I. V Bodnar, G. F. Smirnova, T. V. Smirnova, YU. A. Aleshchenko, and L. K. Vodopyanov, Phys. Status Solidi B **145**, 117 (1988).
[33] A. M. Andrish, N. N. Syrbu, M. S. Iovu, and V. E. Tezlavan, Phys. Status Solidi B **187**, 83 (1995).
[34] N. N. Syrbu, M. Bogdanash, V. E. Tezlevan, and I. Mushcutariu, Physica B **229**, 199 (1997).
[35] R. Márquez and C. Rincón, Phys. Status Solidi B **191**, 115 (1995).
[36] X. Gonze, Ph. Ghosez, and R. W. Godby, Phys. Rev. Lett. **74**, 4035 (1995).
[37] R. M. Martin and G. Ortiz, Phys. Rev. B **56**, 1124 (1997).
[38] Ph. Ghosez, X. Gonze, and R. W. Godby, Phys. Rev. B **56**, 12811 (1997).
[39] I. V Bodnar, A. G. Karoza, and G. F. Smirnova, Phys. Status Solidi B **84**, K65 (1977).
[40] W. Gebicki, J. Filipowicz, and R. Bacewicz, J. Phys.: Condens. Matter **8**, 8695 (1996).
[41] I. V Bodnar, G. F. Smirnova, A. G. Karoza, and A. P. Chernyakova, Phys. Status Solidi B **158**, 469 (1990).

[42] F. J Rámirez and C. Rincón, Solid State Commun. **84**, 551 (1992).
[43] J. González and J. C. Chervin, Jpn. J. Appl. Phys., Suppl. **32-3**, 575 (1993).
[44] K. Wakita, T. Miyazaki, Y. Kikuno, S. Takata, and N. Yamamoto, Jpn. J. Appl. Phys., Part 1 **38**, 664 (1999).
[45] C. Xue, D. Papadimitriou, Y. S. Raptis, N. Esser, W. Richter, S. Siebentritt, and M. Ch. Lux-Steiner, J. Appl. Phys. **94**, 4341 (2003).
[46] C. Rincón and F. J Rámirez, J. Appl. Phys. **72**, 4321 (1992).
[47] I. V Bodnar, L. V. Golubev, V. G. Plotnichhenko, and E. A. Smolyaninova, Phys. Status Solidi B **105**, K111 (1981).
[48] W. R. L Lambrecht, E. Alldredge, and K. Kim, Phys. Rev. B **72**, 155202 (2005).
[49] R. Trommer, E. Anastassakis, and M. Cardona, in *Light Scattering in Solids*, edited by M. Balkanski, R. C. C. Leite, and S. P. S. Porto (Wiley, New York, 1976), p. 396.
[50] G. D. Holah, J. S. Webb, and H. Montgomery, J. Phys. C **7**, 3875 (1974).
[51] A. M. Mintairov, N. A. Sadchikov, T. Sauncy, M. Holtz, G. A. Seryogin, S. A. Nikishin, and H. Temkin, Phys. Rev. B **59**, 15197 (1999).
[52] D. N. Talwar and B. K. Agrawal, Phys. Status Solidi B **64**, 71 (1974).
[53] H. Tanino, T. Maeda, H. Fujikake, H. Nakanishi, S. Endo, and T. Irie, Phys. Rev. B **45**, 13323 (1992).
[54] A. Debernardi and M. Cardona, Phys. Rev. B **54**, 11305 (1996).
[55] R. Trommer, H. Müller, M. Cardona, and P. Vogl, Phys. Rev. B **21**, 4869 (1980).
[56] E. V. Iakovenko, M. Gauthier, and A. Polian, cond-mat/0301045 (unpublished).
[57] K. Kunc and R. M. Martin, Phys. Rev. B **24**, 2311 (1981).